

Higher Order Compact Scheme Combined with Multigrid Method for Momentum, Pressure Poisson and Energy Equations in Cylindrical Geometry

B. Hema Sundar Raju and T.V.S. Sekhar*

Department of Mathematics, Pondicherry Engineering College, Puducherry-605 014, India

Abstract: A higher-order compact scheme combined with the multigrid method is developed for solving Navier-Stokes equations along with pressure Poisson and energy equations in cylindrical polar coordinates. The convection terms in the momentum and energy equations are handled in an effective manner so as to get the fourth order accurate solutions for the flow past a circular cylinder. The superiority of the higher order compact scheme is clearly illustrated in comparison with upwind scheme and defect correction technique by taking a large domain. The developed scheme accurately captures pressure and velocity gradients on the surface when compared to other conventional methods. The pressure in the entire computational domain is computed and the corresponding fourth order accurate pressure fields are plotted. The local Nusselt number and mean Nusselt number are calculated and compared with available experimental and theoretical results.

Keywords: Higher order compact scheme, Navier-stokes equations, Pressure fields, Forced convection and Mean Nusselt number.

1. INTRODUCTION

Higher order compact schemes (HOCS) are invariably applied for Navier Stokes (N-S) equations in cartesian coordinates [1-4] and are applied less to flow problems in curvilinear coordinate systems. Some papers on HOCS in polar coordinates for linear Poisson/quasi-linear Poisson/convection-diffusion equations can be seen in [5-8]. Sanyasiraju and Manjula [9] developed higher order *semi*-compact scheme to incompressible N-S equations in cylindrical coordinates in which compactness is relaxed for some terms. Sengupta *et al.*, [10] analyzed the central and upwind compact schemes and proposed a new optimal upwind based compact scheme. Multigrid methods are more popular to enhance the convergence rate, to use huge mesh points to achieve acceptable accuracy and to reduce computer CPU time and/or memory. To fully investigate the potential of using the fourth-order compact schemes for solving Navier-Stoke's equations, multigrid techniques are more essential. These multigrid methods have been successfully used with first and second-order finite difference methods [11-16]. A preliminary investigation on combining the fourth order compact schemes with multigrid techniques was made by Atlas & Burrage [17] for diffusion dominated flow problems and for Poisson equation Gupta *et al.*, [18]. Multigrid solution and accelerated multigrid solution methods with the fourth order compact schemes for solving convection-dominated problems are relatively new. Some attempts have been made in cartesian coordinates for convection and diffusion equation [19-22] and for Navier-

Stokes equations for a flow in a lid driven cavity [23]. The present paper is concerned with solving the steady two-dimensional Navier-Stokes equations in stream function-vorticity formulation along with pressure Poisson and energy equations using higher order compact scheme (HOCS) combined with multigrid method for the flow past a circular cylinder in cylindrical polar coordinates.

2. BASIC EQUATIONS

Consider the steady-state laminar viscous incompressible flow past a cylinder in a uniform stream with velocity U_∞ from left to right. The governing equations are equation of continuity:

$$\nabla \cdot \mathbf{q} = 0, \quad (1)$$

momentum equation:

$$(\mathbf{q} \cdot \nabla) \mathbf{q} = -\nabla p + \frac{2}{Re} \nabla^2 \mathbf{q} \quad (2)$$

energy equation:

$$\mathbf{q} \cdot \nabla T = \frac{2}{RePr} \nabla^2 T \quad (3)$$

where Re is the Reynolds number defined as

$$Re = \frac{2U_\infty a}{\nu},$$

where a is radius of the cylinder and ν is kinematic coefficient of viscosity. T is the non-dimensionalized temperature, defined by subtracting the main-flow temperature T_∞ from the temperature and dividing by $T_s - T_\infty$ and Pr is the Prandtl number defined as the ratio

*Address correspondence to this author at the Department of Mathematics, Pondicherry Engineering College, Puducherry-605 014, India; Tel: 91-413-2656312; E-mail: sekharhema@pec.edu

between kinematic viscosity (ν) and thermal diffusivity (κ). The non-dimensional radial velocity (q_r) and transverse velocity (q_θ) components (which are obtained by dividing the corresponding dimensional components by the stream velocity U_∞) are chosen in such a way that the equation of continuity (1) is satisfied in cylindrical coordinates. They are

$$q_r = \frac{1}{r} \frac{\partial \psi}{\partial \theta}, \quad q_\theta = -\frac{\partial \psi}{\partial r} \quad (4)$$

2.1. Stream-Function Vorticity Formulation

We have

$$(\mathbf{q} \cdot \nabla) \mathbf{q} = \nabla \left(\frac{1}{2} \mathbf{q}^2 \right) - \mathbf{q} \times (\nabla \times \mathbf{q}) \quad (5)$$

and

$$\nabla \times \nabla \times \mathbf{q} = \nabla (\nabla \cdot \mathbf{q}) - \nabla^2 \mathbf{q} \quad (6)$$

Using equations (5) and (6), the momentum equation (2) becomes

$$\nabla \left(\frac{1}{2} \mathbf{q}^2 \right) - (\mathbf{q} \times \boldsymbol{\omega}) = -\nabla p - \frac{2}{Re} (\nabla \times \boldsymbol{\omega}) \quad (7)$$

where

$$\boldsymbol{\omega} = \nabla \times \mathbf{q} \quad (8)$$

is the vorticity. Taking curl on both sides of the equation (7), we obtain

$$\nabla \times \mathbf{q} \times \boldsymbol{\omega} = \frac{2}{Re} (\nabla \times \nabla \times \boldsymbol{\omega}) \quad (9)$$

Expanding (8) and (9) using (4) with cylindrical coordinates (r, θ, z) (axis-symmetric), we get the Navier-Stokes equations in vorticity-stream function form as

$$\frac{\partial^2 \psi}{\partial r^2} + \frac{1}{r} \frac{\partial \psi}{\partial r} + \frac{1}{r^2} \frac{\partial^2 \psi}{\partial \theta^2} = -\omega$$

and

$$\frac{\partial^2 \omega}{\partial r^2} + \frac{1}{r} \frac{\partial \omega}{\partial r} + \frac{1}{r^2} \frac{\partial^2 \omega}{\partial \theta^2} = \frac{Re}{2} \left(q_r \frac{\partial \omega}{\partial r} + \frac{q_\theta}{r} \frac{\partial \omega}{\partial \theta} \right)$$

Because the stream function and vorticity are expected to vary most rapidly near the surface of the cylinder, we use the transformation $r = e^{\pi \xi}$ and $\theta = \pi \eta$ to concentrate mesh spacing near the body. Now, the above two equations become

$$\frac{\partial^2 \psi}{\partial \xi^2} + \frac{\partial^2 \psi}{\partial \eta^2} + \pi^2 e^{2\pi \xi} \omega = 0 \quad (10)$$

$$\frac{\partial^2 \omega}{\partial \xi^2} + \frac{\partial^2 \omega}{\partial \eta^2} = \frac{Re}{2} \left(\frac{\partial \psi}{\partial \eta} \frac{\partial \omega}{\partial \xi} - \frac{\partial \psi}{\partial \xi} \frac{\partial \omega}{\partial \eta} \right) \quad (11)$$

where ψ and ω are dimensionless stream function and vorticity respectively and

$$q_r = \frac{e^{-\pi \xi}}{\pi} \frac{\partial \psi}{\partial \eta}, \quad q_\theta = \frac{e^{-\pi \xi}}{\pi} \frac{\partial \psi}{\partial \xi}. \quad (12)$$

The boundary conditions to be satisfied are

On the surface of the cylinder

$$(\xi = 0): \psi = \frac{\partial \psi}{\partial \xi} = 0, \quad \omega = -\frac{1}{\pi^2} \frac{\partial^2 \psi}{\partial \xi^2}$$

At large distances from the cylinder

$$(\xi \rightarrow \infty): \psi \sim e^{\pi \xi} \sin \pi \eta, \quad \omega \rightarrow 0$$

Along the axis of symmetry

$$(\eta = 0 \text{ and } \eta = 1): \psi = 0, \quad \omega = 0.$$

The velocity field is obtained by solving equations (10 - 12) using a fourth order compact scheme which is in turn used to solve the following pressure poisson and energy equations.

2.2. Pressure Poisson Equation

Taking divergence on both sides of the momentum equation (2), we obtain

$$\nabla \cdot [(\mathbf{q} \cdot \nabla) \mathbf{q}] = -\nabla^2 p \quad (13)$$

Expanding (13) using equation (4) with cylindrical coordinates (r, θ, z) and apply the transformations $r = e^{\pi \xi}$ and $\theta = \pi \eta$, we obtain pressure poisson equation as follows

$$-\left(\frac{\partial^2 p}{\partial \xi^2} + \frac{\partial^2 p}{\partial \eta^2} \right) = \frac{2e^{-2\pi \xi}}{\pi^2} \left\{ \left(\frac{\partial^2 \psi}{\partial \xi \partial \eta} - \pi \frac{\partial \psi}{\partial \eta} \right)^2 - \left(\frac{\partial^2 \psi}{\partial \xi^2} - \pi \frac{\partial \psi}{\partial \xi} \right) \left(\frac{\partial^2 \psi}{\partial \eta^2} + \pi \frac{\partial \psi}{\partial \xi} \right) \right\} \quad (14)$$

The boundary conditions to be satisfied are

On the surface of the cylinder,

$$(\xi = 0): \frac{\partial p}{\partial \xi} = -\frac{2}{Re} \frac{\partial \omega}{\partial \eta}.$$

At large distances from the cylinder

$$(\xi \rightarrow \infty): p \rightarrow 0,$$

Along the axis of symmetry

$$(\eta = 0 \text{ and } \eta = 1): \frac{\partial p}{\partial \eta} = 0.$$

2.3. Energy Equation

Expanding (3) using equation (4) with cylindrical coordinates (r, θ, z) and apply the transformations $r = e^{\pi \xi}$ and $\theta = \pi \eta$, we obtain energy equation as follows

$$\frac{\partial^2 T}{\partial \xi^2} + \frac{\partial^2 T}{\partial \eta^2} = \frac{RePr}{2} \left(\frac{\partial \psi}{\partial \eta} \frac{\partial T}{\partial \xi} - \frac{\partial \psi}{\partial \xi} \frac{\partial T}{\partial \eta} \right) \quad (15)$$

The boundary conditions for temperature are $T = 1$ on the surface of the cylinder, $T \rightarrow 0$ as $\xi \rightarrow \infty$ and $\frac{\partial T}{\partial \eta} = 0$ along the axis of symmetry.

3. FOURTH ORDER COMPACT SCHEME

The standard fourth order central difference operator of the first and second order partial derivatives are given by the following equations

$$\frac{\partial \varphi}{\partial \xi} = \delta_{\xi} \varphi - \frac{h^2}{6} \frac{\partial^3 \varphi}{\partial \xi^3} + O(h^4) \tag{16}$$

$$\frac{\partial^2 \varphi}{\partial \xi^2} = \delta_{\xi}^2 \varphi - \frac{h^2}{12} \frac{\partial^4 \varphi}{\partial \xi^4} + O(h^4) \tag{17}$$

$$\frac{\partial \varphi}{\partial \eta} = \delta_{\eta} \varphi - \frac{k^2}{6} \frac{\partial^3 \varphi}{\partial \eta^3} + O(k^4) \tag{18}$$

$$\frac{\partial^2 \varphi}{\partial \eta^2} = \delta_{\eta}^2 \varphi - \frac{k^2}{12} \frac{\partial^4 \varphi}{\partial \eta^4} + O(k^4) \tag{19}$$

where $\delta_{\xi} \varphi$, $\delta_{\xi}^2 \varphi$, $\delta_{\eta} \varphi$ and $\delta_{\eta}^2 \varphi$ are standard second order central discretizations such that

$$\delta_{\xi} \varphi_{i,j} = \frac{\varphi_{i+1,j} - \varphi_{i-1,j}}{2h}$$

$$\delta_{\xi}^2 \varphi_{i,j} = \frac{\varphi_{i+1,j} - 2\varphi_{i,j} + \varphi_{i-1,j}}{h^2}$$

$$\delta_{\eta} \varphi_{i,j} = \frac{\varphi_{i,j+1} - \varphi_{i,j-1}}{2k}$$

$$\delta_{\eta}^2 \varphi_{i,j} = \frac{\varphi_{i,j+1} - 2\varphi_{i,j} + \varphi_{i,j-1}}{k^2}$$

3.1. Discretization of Momentum Equation

Using (17) and (19) in equation (10), we obtain

$$-\delta_{\xi}^2 \psi_{i,j} - \delta_{\eta}^2 \psi_{i,j} + s_{i,j} - \chi_{i,j} = 0 \tag{20}$$

The truncation error of equation (20) is

$$\chi_{i,j} = - \left[\left(\frac{h^2}{12} \frac{\partial^4 \psi}{\partial \xi^4} + \frac{k^2}{12} \frac{\partial^4 \psi}{\partial \eta^4} \right) \right]_{i,j} + O(h^4, k^4) \tag{21}$$

and

$$s_{i,j} = -(\pi^2 e^{2\pi\xi} \omega)_{i,j}$$

Differentiating partially the stream-function equation (10) twice on both sides with respect to ξ and η , we obtain the following equations

$$\frac{\partial^3 \psi}{\partial \xi^3} = - \frac{\partial^3 \psi}{\partial \xi \partial \eta^2} + \frac{\partial s}{\partial \xi} \tag{22}$$

$$\frac{\partial^4 \psi}{\partial \xi^4} = - \frac{\partial^4 \psi}{\partial \xi^2 \partial \eta^2} + \frac{\partial^2 s}{\partial \xi^2} \tag{23}$$

$$\frac{\partial^3 \psi}{\partial \eta^3} = - \frac{\partial^3 \psi}{\partial \xi^2 \partial \eta} + \frac{\partial s}{\partial \eta} \tag{24}$$

$$\frac{\partial^4 \psi}{\partial \eta^4} = - \frac{\partial^4 \psi}{\partial \xi^2 \partial \eta^2} + \frac{\partial^2 s}{\partial \eta^2} \tag{25}$$

Using equations (21), (23) and (25) in equation (20), we obtain

$$-\delta_{\xi}^2 \psi_{i,j} - \delta_{\eta}^2 \psi_{i,j} - \left(\frac{h^2 + k^2}{12} \right) \delta_{\xi}^2 \delta_{\eta}^2 \psi_{i,j} + \tag{26}$$

$$\frac{h^2}{12} \delta_{\xi}^2 s_{i,j} + \frac{k^2}{12} \delta_{\eta}^2 s_{i,j} + s_{i,j} = 0$$

Equation (26) is the fourth order compact discretization of the governing equation (10). Equation (11) is rewritten as

$$-\frac{\partial^2 \omega}{\partial \xi^2} - \frac{\partial^2 \omega}{\partial \eta^2} + c \frac{\partial \omega}{\partial \xi} + d \frac{\partial \omega}{\partial \eta} = 0 \tag{27}$$

where

$$c = \frac{Re}{2} \frac{\partial \psi}{\partial \eta},$$

$$d = - \frac{Re}{2} \frac{\partial \psi}{\partial \xi}.$$

Once again using (16) - (19) in equation (27), we obtain

$$-\delta_{\xi}^2 \omega_{i,j} - \delta_{\eta}^2 \omega_{i,j} + c_{i,j} \delta_{\xi} \omega_{i,j} + d_{i,j} \delta_{\eta} \omega_{i,j} - \tau_{i,j} = 0. \tag{28}$$

The truncation error of equation (28) is

$$\tau_{i,j} = \left[\begin{aligned} &2 \left(\frac{h^2}{12} c \frac{\partial^3 \omega}{\partial \xi^3} + \frac{k^2}{12} d \frac{\partial^3 \omega}{\partial \eta^3} \right) - \\ &\left(\frac{h^2}{12} \frac{\partial^4 \omega}{\partial \xi^4} + \frac{k^2}{12} \frac{\partial^4 \omega}{\partial \eta^4} \right) \end{aligned} \right]_{i,j} + O(h^4, k^4), \tag{29}$$

where h and k are grid spacing ($h \neq k$) in the radial and angular directions, respectively. Differentiating partially the vorticity equation (27) twice with respect to ξ and η , we obtain the following equations

$$\frac{\partial^3 \omega}{\partial \xi^3} = - \frac{\partial^3 \omega}{\partial \xi \partial \eta^2} + c \frac{\partial^2 \omega}{\partial \xi^2} + d \frac{\partial^2 \omega}{\partial \xi \partial \eta} + \frac{\partial c}{\partial \xi} \frac{\partial \omega}{\partial \xi} + \frac{\partial d}{\partial \xi} \frac{\partial \omega}{\partial \eta} \tag{30}$$

$$\begin{aligned} \frac{\partial^4 \omega}{\partial \xi^4} = & - \frac{\partial^4 \omega}{\partial \xi^2 \partial \eta^2} - c \frac{\partial^3 \omega}{\partial \xi \partial \eta^2} + d \frac{\partial^3 \omega}{\partial \xi^2 \partial \eta} + \\ & \left(2 \frac{\partial c}{\partial \xi} + c^2 \right) \frac{\partial^2 \omega}{\partial \xi^2} + \left(2 \frac{\partial d}{\partial \xi} + cd \right) \frac{\partial^2 \omega}{\partial \xi \partial \eta} + \\ & \left(\frac{\partial^2 c}{\partial \xi^2} + c \frac{\partial c}{\partial \xi} \right) \frac{\partial \omega}{\partial \xi} + \left(\frac{\partial^2 d}{\partial \xi^2} + c \frac{\partial d}{\partial \xi} \right) \frac{\partial \omega}{\partial \eta} \end{aligned} \tag{31}$$

$$\frac{\partial^3 \omega}{\partial \eta^3} = - \frac{\partial^3 \omega}{\partial \xi^2 \partial \eta} + c \frac{\partial^2 \omega}{\partial \xi \partial \eta} + d \frac{\partial^2 \omega}{\partial \eta^2} + \frac{\partial c}{\partial \eta} \frac{\partial \omega}{\partial \xi} + \frac{\partial d}{\partial \eta} \frac{\partial \omega}{\partial \eta} \tag{32}$$

$$\begin{aligned} \frac{\partial^4 \omega}{\partial \eta^4} = & - \frac{\partial^4 \omega}{\partial \xi^2 \partial \eta^2} + c \frac{\partial^3 \omega}{\partial \xi \partial \eta^2} - d \frac{\partial^3 \omega}{\partial \xi^2 \partial \eta} + \\ & \left(2 \frac{\partial d}{\partial \eta} + d^2 \right) \frac{\partial^2 \omega}{\partial \eta^2} + \left(2 \frac{\partial c}{\partial \eta} + cd \right) \frac{\partial^2 \omega}{\partial \xi \partial \eta} + \\ & \left(\frac{\partial^2 c}{\partial \eta^2} + d \frac{\partial c}{\partial \eta} \right) \frac{\partial \omega}{\partial \xi} + \left(\frac{\partial^2 d}{\partial \eta^2} + d \frac{\partial d}{\partial \eta} \right) \frac{\partial \omega}{\partial \eta} \end{aligned} \tag{33}$$

Substituting equations (29) - (33) in equation (28) gives

$$-e_{i,j}\delta_\xi^2\omega_{i,j} - f_{i,j}\delta_\eta^2\omega_{i,j} + g_{i,j}\delta_\xi\delta_\eta\omega_{i,j} + o_{i,j}\delta_\eta\omega_{i,j} + l_{i,j}\delta_\xi\delta_\eta\omega_{i,j} - \left(\frac{h^2+k^2}{12}\right)(\delta_\xi^2\delta_\eta^2\omega_{i,j} - c_{i,j}\delta_\xi\delta_\eta^2\omega_{i,j} - d_{i,j}\delta_\xi^2\delta_\eta\omega_{i,j}) = 0 \quad (34)$$

where the coefficients $e_{i,j}$, $f_{i,j}$, $g_{i,j}$, $o_{i,j}$ and $l_{i,j}$ are given by

$$\begin{aligned} e_{i,j} &= 1 + \frac{h^2}{12}(c_{i,j}^2 - 2\delta_\xi c_{i,j}) \\ f_{i,j} &= 1 + \frac{k^2}{12}(d_{i,j}^2 - 2\delta_\eta d_{i,j}) \\ g_{i,j} &= c_{i,j} + \frac{h^2}{12}(\delta_\xi^2 c_{i,j} - c_{i,j}\delta_\xi c_{i,j}) + \frac{k^2}{12}(\delta_\eta^2 c_{i,j} - d_{i,j}\delta_\eta c_{i,j}) \\ o_{i,j} &= d_{i,j} + \frac{h^2}{12}(\delta_\xi^2 d_{i,j} - c_{i,j}\delta_\xi d_{i,j}) + \frac{k^2}{12}(\delta_\eta^2 d_{i,j} - d_{i,j}\delta_\eta d_{i,j}) \\ l_{i,j} &= \frac{h^2}{6}\delta_\xi d_{i,j} + \frac{k^2}{6}\delta_\eta c_{i,j} - \left(\frac{h^2+k^2}{12}\right)c_{i,j}d_{i,j} \end{aligned}$$

Equation (34) is the fourth order compact discretization of the governing equation (11). The fourth order compact differences for the coefficients c and d are given by

$$\begin{aligned} c &= \frac{Re}{2} \left(\delta_\eta \psi - \frac{k^2}{6} \frac{\partial^3 \psi}{\partial \eta^3} \right) \\ d &= -\frac{Re}{2} \left(\delta_\xi \psi - \frac{h^2}{6} \frac{\partial^3 \psi}{\partial \xi^3} \right) \end{aligned}$$

3.2. Discretization of Pressure Poisson Equation

Equation (14) is rewritten as

$$-\frac{\partial^2 p}{\partial \xi^2} - \frac{\partial^2 p}{\partial \eta^2} = F_{i,j} \quad (35)$$

where

$$F_{i,j} = \left[\frac{2e^{-2\pi\xi}}{\pi^2} \left\{ \left(\frac{\partial^2 \psi}{\partial \xi \partial \eta} - \pi \frac{\partial \psi}{\partial \eta} \right)^2 - \left(\frac{\partial^2 \psi}{\partial \xi^2} - \pi \frac{\partial \psi}{\partial \xi} \right) \left(\frac{\partial^2 \psi}{\partial \eta^2} + \pi \frac{\partial \psi}{\partial \xi} \right) \right\} \right]_{i,j} \quad (36)$$

Again using equations (17) and (19) in equation (35), we obtain

$$-\delta_\xi^2 p_{i,j} - \delta_\eta^2 p_{i,j} + \Omega_{i,j} - F_{i,j} = 0. \quad (37)$$

The truncation error of equation (37) is

$$\Omega_{i,j} = \left[\frac{h^2}{12} \frac{\partial^4 p}{\partial \xi^4} + \frac{k^2}{12} \frac{\partial^4 p}{\partial \eta^4} \right]_{i,j} + O(h^4, k^4) \quad (38)$$

Differentiating partially the poisson equation (35) twice with respect to ξ and η , we obtain the following equations

$$\frac{\partial^4 p}{\partial \xi^4} = -\frac{\partial^4 p}{\partial \xi^2 \partial \eta^2} - \frac{\partial^2 F}{\partial \xi^2} \quad (39)$$

$$\frac{\partial^4 p}{\partial \eta^4} = -\frac{\partial^4 p}{\partial \xi^2 \partial \eta^2} - \frac{\partial^2 F}{\partial \eta^2} \quad (40)$$

Using equations (38) - (40) in equation (37), we obtain

$$-\delta_\xi^2 p_{i,j} - \delta_\eta^2 p_{i,j} - \left(\frac{h^2+k^2}{12}\right)\delta_\xi^2\delta_\eta^2 p_{i,j} = \frac{h^2}{12}\delta_\xi^2 F_{i,j} + \frac{k^2}{12}\delta_\eta^2 F_{i,j} + F_{i,j} \quad (41)$$

Equation (41) is the fourth order approximation to pressure poisson equation (35).

3.3. Discretization of Energy Equation

Equation (15) is rewritten as

$$-\frac{\partial^2 T}{\partial \xi^2} - \frac{\partial^2 T}{\partial \eta^2} + a \frac{\partial T}{\partial \xi} + b \frac{\partial T}{\partial \eta} = 0 \quad (42)$$

where

$$\begin{aligned} a &= \frac{RePr}{2} \frac{\partial \psi}{\partial \eta}, \\ b &= -\frac{RePr}{2} \frac{\partial \psi}{\partial \xi}. \end{aligned}$$

Repeating the above discretization process of the vorticity equation (27) to energy equation (42), we obtain

$$\begin{aligned} -\alpha_{i,j}\delta_\xi^2 T_{i,j} - \beta_{i,j}\delta_\eta^2 T_{i,j} + \gamma_{i,j}\delta_\xi T_{i,j} + \lambda_{i,j}\delta_\eta T_{i,j} + \mu_{i,j}\delta_\xi\delta_\eta T_{i,j} - \left(\frac{h^2+k^2}{12}\right)(\delta_\xi^2\delta_\eta^2 T_{i,j} - a_{i,j}\delta_\xi\delta_\eta^2 T_{i,j} - b_{i,j}\delta_\xi^2\delta_\eta T_{i,j}) = 0 \quad (43) \end{aligned}$$

where the coefficients $\alpha_{i,j}$, $\beta_{i,j}$, $\gamma_{i,j}$, $\lambda_{i,j}$ and $\mu_{i,j}$ are given by

$$\begin{aligned} \alpha_{i,j} &= 1 + \frac{h^2}{12}(a_{i,j}^2 - 2\delta_\xi a_{i,j}) \\ \beta_{i,j} &= 1 + \frac{k^2}{12}(b_{i,j}^2 - 2\delta_\eta b_{i,j}) \\ \gamma_{i,j} &= a_{i,j} + \frac{h^2}{12}(\delta_\xi^2 a_{i,j} - a_{i,j}\delta_\xi a_{i,j}) + \frac{k^2}{12}(\delta_\eta^2 a_{i,j} - b_{i,j}\delta_\eta a_{i,j}) \\ \lambda_{i,j} &= b_{i,j} + \frac{h^2}{12}(\delta_\xi^2 b_{i,j} - a_{i,j}\delta_\xi b_{i,j}) + \frac{k^2}{12}(\delta_\eta^2 b_{i,j} - b_{i,j}\delta_\eta b_{i,j}) \\ \mu_{i,j} &= \frac{h^2}{6}\delta_\xi b_{i,j} + \frac{k^2}{6}\delta_\eta a_{i,j} - \left(\frac{h^2+k^2}{12}\right)a_{i,j}b_{i,j} \end{aligned}$$

Equation (43) is the fourth order approximation to energy equation (42).

The fourth order compact differences for the coefficients a and b are given by

$$\begin{aligned} a &= \frac{RePr}{2} \left(\delta_\eta \psi - \frac{k^2}{6} \frac{\partial^3 \psi}{\partial \eta^3} \right) \\ b &= -\frac{RePr}{2} \left(\delta_\xi \psi - \frac{h^2}{6} \frac{\partial^3 \psi}{\partial \xi^3} \right) \end{aligned}$$

The two-dimensional cross derivative central difference operators on a uniform anisotropic mesh ($h \neq k$) are given by

$$\begin{aligned}\delta_\xi \delta_\eta \varphi_{i,j} &= \frac{\varphi_{i+1,j+1} - \varphi_{i+1,j-1} - \varphi_{i-1,j+1} + \varphi_{i-1,j-1}}{4hk} \\ \delta_\xi^2 \delta_\eta \varphi_{i,j} &= \frac{\varphi_{i+1,j+1} - \varphi_{i+1,j-1} + \varphi_{i-1,j+1} - \varphi_{i-1,j-1} - 2\varphi_{i,j+1} + 2\varphi_{i,j-1}}{2h^2k} \\ \delta_\xi \delta_\eta^2 \varphi_{i,j} &= \frac{\varphi_{i+1,j+1} - \varphi_{i-1,j+1} + \varphi_{i+1,j-1} - \varphi_{i-1,j-1} + 2\varphi_{i,j} - 2\varphi_{i+1,j}}{2hk^2} \\ \delta_\xi^2 \delta_\eta^2 \varphi_{i,j} &= \frac{\varphi_{i+1,j+1} + \varphi_{i+1,j-1} + \varphi_{i-1,j+1} + \varphi_{i-1,j-1} - 2\varphi_{i,j+1} - 2\varphi_{i,j-1} - 2\varphi_{i+1,j} - 2\varphi_{i-1,j} + 4\varphi_{i,j}}{h^2k^2}\end{aligned}$$

where $\varphi = \psi$ or ω or p or T .

3.4. Discretization of Boundary Conditions

On the surface of the cylinder, no-slip condition is applied. At far off distances ($\xi \rightarrow \infty$) uniform flow is imposed. We now turn to the boundary condition for the vorticity, focusing our discussion on the boundary where $i = 1$. The vorticity boundary condition at $i = 1$ is derived using $\psi = \frac{\partial \psi}{\partial \xi} = 0$ in equation (10). Following Briley's procedure [24] we obtain the formula

$$\omega_{1,j} = -\frac{(108\psi_{2,j} - 27\psi_{3,j} + 4\psi_{4,j})}{18h^2\pi^2} \quad (44)$$

For evaluating boundary conditions, along the axis of symmetry, the derivative $\frac{\partial \varphi}{\partial \theta}$ is approximated by fourth order forward difference along $\theta = 0$ (i.e., $j = 1$) and fourth order backward difference along $\theta = \pi$ (or $j = m + 1$) as follows.

$$\begin{aligned}\varphi(i,1) &= \frac{1}{25} [48\varphi(i,2) - 36\varphi(i,3) + 16\varphi(i,4) - 3\varphi(i,5)] \\ \varphi(i,m+1) &= \frac{1}{25} [48\varphi(i,m) - 36\varphi(i,m-1) + 16\varphi(i,m-2) - 3\varphi(i,m-3)]\end{aligned}$$

where $\varphi = p$ or T .

4. MULTIGRID METHOD WITH COARSEGRID CORRECTION

To enhance the convergence rate of HOCS discretization, multigrid technique with coarse grid correction has been used with five grids namely 16×16 (coarsest), 32×32 , 64×64 , 128×128 and 256×256 (finest). The restriction operator R_k^{k-1} transfers a fine grid function U^k to a coarse grid function U^{k-1} , while the prolongation operator denoted by P_{k-1}^k , transfers a coarse grid function U^{k-1} to a fine grid function U^k . In this study $k = 5$ is the finest grid 256×256 . The restriction operator used in this study is

injection where by the values of a function in the coarse grid are taken to be exactly the values at the corresponding points of the next fine grid i.e.,

$$(R_k^{k-1}u^k)_{i+1,j+1} = u_{2i+1,2j+1}^k$$

The following 9-point prolongation operator derived by using linear interpolation is used for the present study [25].

$$(P_{k-1}^k u^{k-1})_{2i+1,2j+1} = u_{i+1,j+1}^{k-1}$$

$$(P_{k-1}^k u^{k-1})_{2i+2,2j+1} = \frac{1}{2} (u_{i+1,j+1}^{k-1} + u_{i+2,j+1}^{k-1})$$

$$(P_{k-1}^k u^{k-1})_{2i+1,2j+2} = \frac{1}{2} (u_{i+1,j+1}^{k-1} + u_{i+1,j+2}^{k-1})$$

$$(P_{k-1}^k u^{k-1})_{2i+2,2j+2} = \frac{1}{4} (u_{i+1,j+1}^{k-1} + u_{i+1,j+2}^{k-1} + u_{i+2,j+1}^{k-1} + u_{i+2,j+2}^{k-1}).$$

It is known that the role of the iterative relaxation scheme in the multigrid method is to eliminate the high-frequency error components. Due to the coupling between the discretized governing equations (26) and (34), as well as through the discretized vorticity boundary condition (44), sequential relaxation of the individual equations (26) and (34) will have poor smoothing rate. Smoothing errors in ω using equation (34) will produce high-frequency error components in the vorticity solution via the boundary condition (44). In brief, a convergent solution of each equation at each step will constitute a very inefficient procedure [11]. Hence in the present study, the coupled governing equations (26) and (34) are relaxed simultaneously and the vorticity boundary condition is incorporated implicitly. A coupled point Gauss-Seidel procedure is used for this purpose. For example with a two-grid computation, each iteration of the multigrid algorithm is carried out as follows:

- Perform few pre-smoothing (Point Gauss-Seidel) iterations on finest grid.
- Compute Residual.
- Restrict Residual (*fine* \rightarrow *coarse*).
- Solve the error equation on coarsest grid.
- Prolongate the error (*coarse* \rightarrow *fine*).
- Correct the solution.
- Perform few post-smoothing (Point Gauss-Seidel) iterations and repeat the above process.

The iterations are continued until the norm of the dynamic residuals is less than 10^{-5} .

5. RESULTS AND DISCUSSION

A large far field of 120.023 times the radius of the cylinder is considered in all the numerical simulations. The drag coefficient C_D is defined by the equation

$$C_D = \frac{D}{\pi \rho U_\infty^2 a^2},$$

where D is the total drag on the cylinder, a is the radius of the cylinder and ρ is the density of the fluid. The drag coefficient is composed of two parts due to the viscous and pressure drag, respectively. The viscous drag coefficient is given by

$$C_v = -\frac{4\pi}{Re} \int_0^1 \omega(0, \eta) \sin(\pi\eta) d\eta,$$

and the pressure drag coefficient is

$$C_p = \frac{4}{Re} \int_0^1 \left(\frac{\partial \omega}{\partial \xi} \right)_{\xi=0} \sin(\pi\eta) d\eta,$$

The total drag coefficient, $C_D = C_v + C_p$. The drag coefficient values obtained from different grids for $Re = 20$ and 40 are tabulated in Table 1 to show grid independence. It is clear from the Table 1 that (i) the solutions obtained from the present numerical scheme exhibit grid independence, and (ii) fourth order compact scheme provide accurate results even with a computationally inexpensive 64×64 grid.

Calculated fourth order accurate separation length (L), separation angle (θ_s) and drag coefficient values for $Re = 20$ and 40 are given in Table 2 along with other literature values of Sanyasiraju & Manjula [9], Dennis & Chang [26], Fornberg [27], He & Doolen [28], Niu *et al.*, [29] and with experimental results of Tritton [30]. The results concur with all literature values including the recent values predicted by Sanyasiraju & Manjula [9].

It is well known that, for the convection-dominated problems, approximating the derivatives by the five-point second-order central difference scheme (CDS) has a truncation error of order $O(h^2)$ but may produce nonphysical oscillations for large Re . Approximating second order derivatives by central differences and convective terms by upwind scheme (UDS) prevents oscillations but reduces the order of accuracy to $O(h)$. The results obtained by UDS can be extended to second order accuracy by applying defect

correction technique (DC) [14]. In this study, the results are also simulated with UDS and DC techniques with a large domain of 120.023 times the radius of the cylinder and compared with HOCS. The drag coefficients at $Re = 40$ in different grids are compared with the UDS and DC technique in Table 3. It can be verified from the table that the results obtained from UDS and DC are not grid independent even in 256×256 grid and hence the results are simulated over a high resolution grid of 512×512 , whereas HOCS achieves grid independence in a 64×64 grid. It is observed that the smallest possible grid for convergence of upwind scheme and DC at $Re = 40$ is 128×128 , while for fourth order HOCS, it is 16×16 . It is evident from Table 3 that DC technique improves the accuracy of the solution in comparison with UDS and the solutions obtained by both the schemes can be achieved by the computationally inexpensive 32×32 grid by HOCS. This clearly illustrates the superiority of HOCS in comparison with upwind scheme and DC technique and can be concluded as follows. (i) HOCS can be used in large domains (ii) HOCS gives convergence even in coarser grids (iii) Results obtained by upwind scheme and DC technique in finer grids can be achieved by HOCS in coarser grids.

The surface pressure is calculated using the following relations:

$$p(\xi = 0, \theta = \pi) = 1 - \frac{4}{\pi Re} \int_0^\infty \left(\frac{\partial \omega}{\partial \eta} \right)_{\eta=1} d\xi \quad (45)$$

and

$$p(\xi = 0, \theta) = 1 - \frac{4}{\pi Re} \int_0^\infty \left(\frac{\partial \omega}{\partial \eta} \right)_{\eta=1} d\xi - \frac{4}{Re} \int_\eta^1 \left(\frac{\partial \omega}{\partial \xi} \right)_{\xi=0} d\eta. \quad (46)$$

The surface pressure obtained by the above formula is presented in Fig. (1a). The surface vorticity is also presented in Fig. (1b). The pattern of these graphs is in good agreement with those presented by Dennis and Chang [26] and Fornberg [27]. The surface pressure at front and rear

Table 1. Grid independence of Fourth Order Accurate Drag Coefficient Values

Re	16×16	32×32	48×48	64×64	96×96	128×128
20	1.67429	1.96844	2.01082	2.01832	2.02040	2.02049
40	0.89796	1.32116	1.45845	1.49321	1.50762	1.50965

Table 2. Comparison of Separation Length, Separation Angle and Drag Coefficient Values with Literature for $Re = 20, 40$

	Re	Ref. [26]	Ref. [27]	Ref. [28]	Ref. [9]	Ref. [29]	Ref. [30]	Present Results
L	20	1.88	1.82	1.842	1.77	1.92	--	1.797
	40	4.69	4.48	4.49	4.21	4.51	--	4.383
θ_s	20	43.7	42.9	42.96	41.328	42.79	--	42.891
	40	53.8	51.5	52.84	51.025	52.84	--	52.734
C_D	20	2.045	2.001	2.152	2.060	2.111	2.05	2.020
	40	1.522	1.498	1.499	1.530	1.574	1.57	1.510

Table 3. Comparison of HOCS Drag Coefficient Values with UDS and DC Technique for $Re = 40$. Here NC Means No Convergence

<i>Scheme</i>	16×16	32×32	64×64	128×128	256×256	512×512	L	θ_s
<i>UDS</i>	NC	NC	NC	1.228	1.365	1.437	4.69	53.08
<i>DC</i>	NC	NC	NC	1.232	1.368	1.439	4.69	53.08
<i>HOCS</i>	0.898	1.321	1.493	1.510	1.510	--	4.38	52.73

Table 4. Comparison of Pressure at Front and Rear Stagnation Points Obtained from the Relations (45) & (46) and Pressure Poisson Equation with Other Literature Values.

Re	Ref. [26]		Ref. [27]		Using (45) & (46)		Poisson Equation	
	$p(0)$	$p(\pi)$	$p(0)$	$p(\pi)$	$p(0)$	$p(\pi)$	$p(0)$	$p(\pi)$
5	-1.044	1.872	--	--	-0.977	1.851	-0.954	1.874
7	-0.870	1.660	--	--	-0.821	1.645	-0.802	1.665
10	-0.742	1.489	--	--	-0.702	1.482	-0.686	1.497
20	-0.589	1.269	-0.54	1.28	-0.565	1.266	-0.555	1.274
40	-0.509	1.144	-0.46	1.14	-0.493	1.143	-0.491	1.142

stagnation points of the cylinder are in line with the results of Dennis & Chang [26] and Fornberg [27] as shown in Table 4.

The separation occurs initially at $Re = 6.5$ and the separation point increases with increase of Re as expected. This is due to the increase of adverse pressure gradient in the out flow region with increase of Re as illustrated in Fig. (2a). The transverse velocity gradients in the radial direction on the surface of the cylinder is presented in Fig. (2b) for $0 < Re \leq 40$, in which the point $\frac{\partial q_\theta}{\partial r} = 0$ indicates the point of separation. The radial velocity gradient in the radial direction on the surface of the cylinder is also presented in Fig. (2c) wherein $\frac{\partial q_r}{\partial r} < 0$ in the wake region. To understand the superiority of the HOCS, the pressure, radial and transverse velocity gradients are computed on the surface of the cylinder and compared with upwind scheme and defect correction technique at $Re = 40$ as shown in Fig. (3a-c). It can be verified from Fig. (3a) that the HOCS captures pressure gradients up to the lowest value than other schemes. It can be noted from Fig. (3b) that the radial velocity gradient differs significantly with HOCS although there is not much difference in transverse velocity gradient (Fig. 3c). This difference resulted in slightly higher separation length 4.69 units and separation angle 53.08° for $Re = 40$ by upwind and DC techniques and significantly differs in drag coefficient as shown in Table 3.

The pressure is computed in the entire computational domain by solving pressure Poisson equation using HOCS and the fourth order accurate pressure fields are presented in Fig. (4a, b) for $Re = 5$ and 40 respectively. The surface pressure at front and rear stagnation points obtained from the pressure Poisson equation is also presented in the Table 4.

These values are reasonably in good agreement with those obtained from vorticity (Relations (45) & (46)) and also with other literature values.

The heat transfer due to forced convection from a circular cylinder is analyzed by solving energy equation using HOCS on the nine point 2-D stencil. Numerical investigations were carried out for the Reynolds numbers in the range $1 \leq Re \leq 40$ and different values of Prandtl numbers (Pr) such that the Peclet number ($Pe = Re.Pr$) is restricted to 400. The heat flux $q(\eta)$ from the cylinder to the fluid is computed using

$$q(\eta) = -k \frac{T_s - T_\infty}{\pi a} \left(\frac{\partial T}{\partial \xi} \right)_{\xi=0}$$

where k is the thermal conductivity. The local Nusselt number is defined by

$$Nu(\eta) = \frac{2aq(\eta)}{k(T_s - T_\infty)} = -\frac{2}{\pi} \left(\frac{\partial T}{\partial \xi} \right)_{\xi=0} \quad (47)$$

and the mean Nusselt number as

$$N_m = \int_0^1 Nu(\eta) d\eta. \quad (48)$$

In equations (47) and (48) the derivative $\frac{\partial T}{\partial \xi}$ is approximated with fourth order finite differences. The calculated fourth order accurate mean Nusselt number values in the range $1 \leq Re \leq 40$ for $Pr = 0.73$ are compared with the results of Kramers [31], Zijnen [32], Dennis *et al.*, [33] and Lange *et al.*, [34] in Fig. (5). The results are in agreement with the numerical results of Dennis *et al.*, and the recent results of Lange *et al.*, The calculated mean

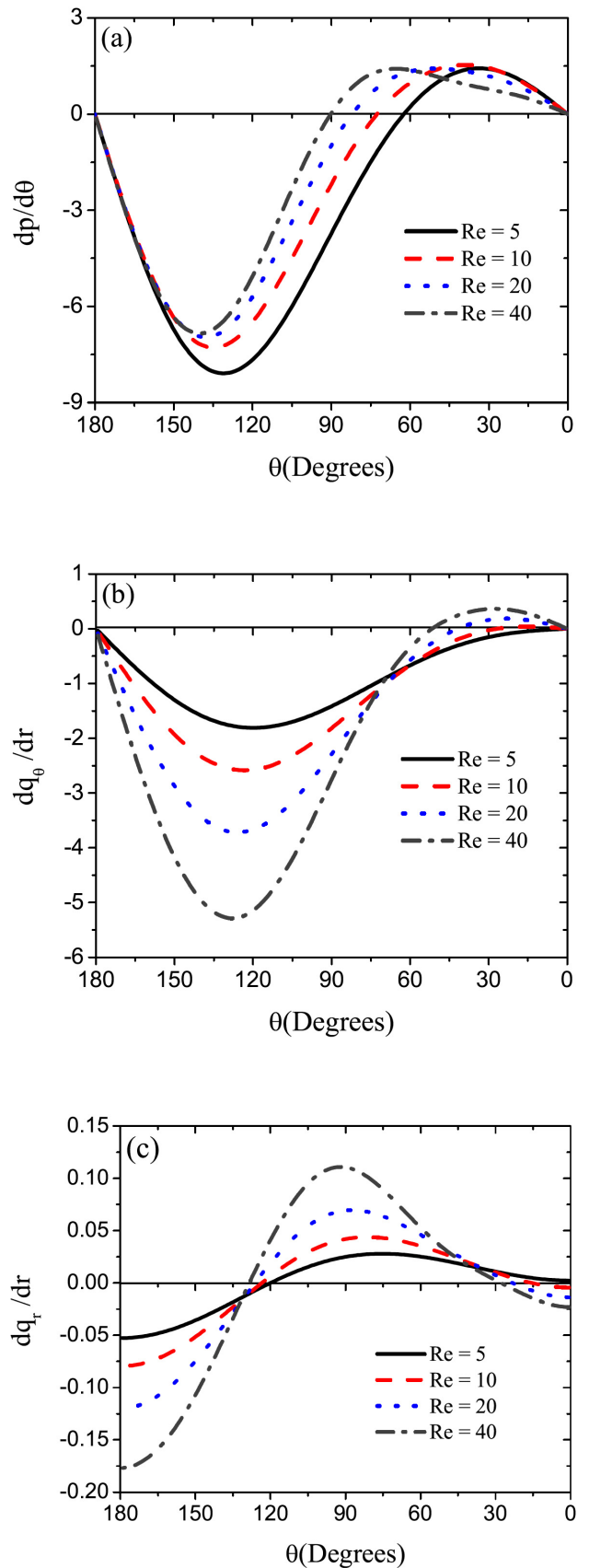
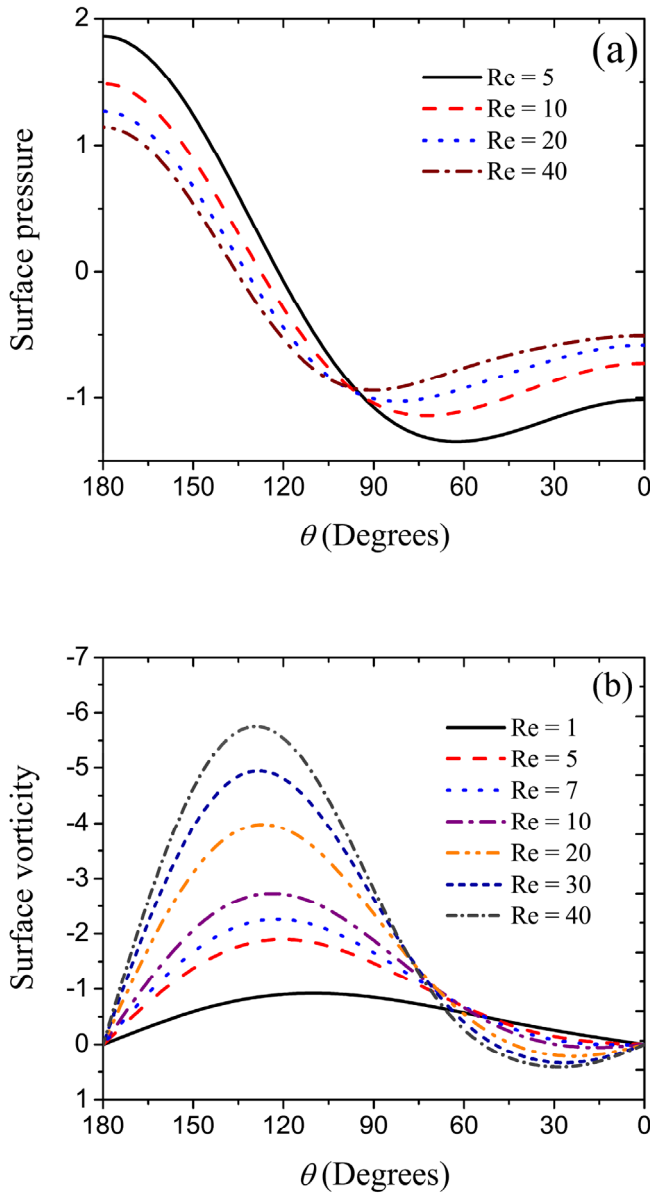


Fig. (1). (a) Angular variation of the surface pressure for different Re and (b) Angular variation of the surface vorticity for different Re .

Nusselt number values for $Re = 2$ at $Pr = 50$ and for $Re = 20$ at $Pr = 5$ are compared with the results of Kramers [31], Kurdyumov & Fernandez [35] and Juncu [36] in Table 5. The results agree with the results of Kurdyumov & Fernandez and the recent numerical results of Juncu.

The dependance of mean Nusselt number on Re and Pr are presented in Fig. (6). As Re or Pr increases, the mean Nusselt number increases as expected. The mean Nusselt number N_m is found to vary with \sqrt{Re} . This behavior can be seen in Fig. (7). The Colburn heat transfer factor (j) is calculated using the formula

$$j = \frac{N_m}{Re(Pr^{1/3})}$$

Fig. (2). Angular variation of (a) pressure gradient (b) transverse velocity gradient (c) radial velocity gradient for different Re on the surface of the cylinder.

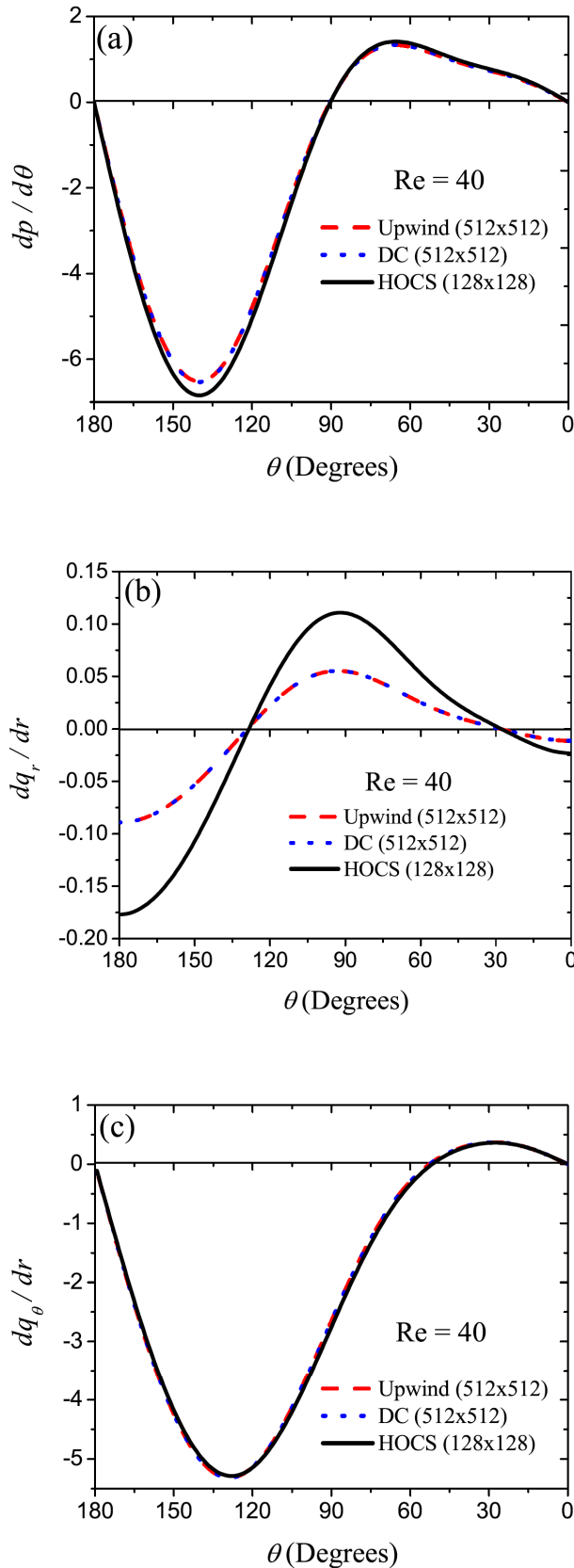


Fig. (3). Comparison of angular variation of (a) Pressure gradient (b) radial velocity gradient (c) transverse velocity gradient along the surface of the cylinder with other schemes.

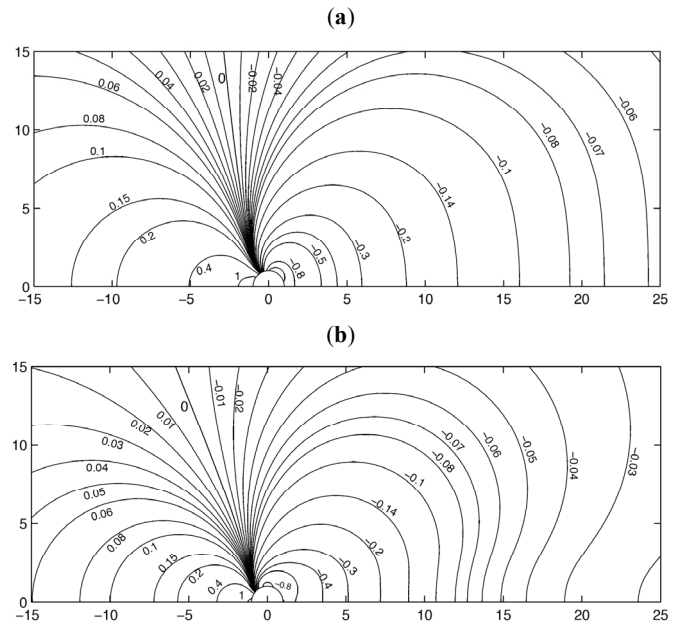


Fig. (4). Fourth order accurate pressure fields for (a) $Re = 5$ and (b) $Re = 40$.

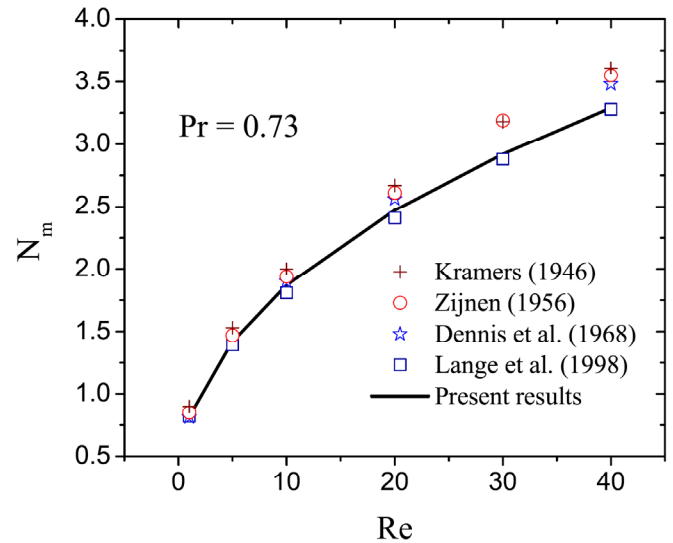


Fig. (5). Comparison of fourth order accurate mean Nusselt number N_m values with other experimental and theoretical results for various Re with $Pr = 0.73$.

Fig. (8) shows that Colburn heat transfer factor (j) varies linearly with Re on log-log scale [37]. The angular variation of local Nusselt number on the surface of the cylinder is presented for $Re = 5, 40$ with various values of Pr ; and for $Pr = 1, 10$ with various values of Re in Fig. (9). At low Re ($Re < 20$), the local Nusselt number decreases along the surface of the cylinder [33, 38], where as for $Re \geq 20$, the local Nusselt number decreases along the surface of the cylinder until it reaches near the point of separation beyond which it increases in the far downstream [39, 40]. This is due to the separation and reversal of flow. It can also be noted that the maximum heat transfer takes place near the front stagnation point $\theta = \pi$ (Fig. 9).

Table 5. Comparison of N_m Values for $Re = 2, Pr = 50$ and $Re = 20, Pr = 5$ with the Literature Values

Re	Pr	N_m	Authors
2	50	3.8881	Kramers [31]
		3.6314	Kurdyumov & Fernandez [35]
		3.5930	Juncu [36]
		3.6182	Present
20	5	4.9384	Kramers [31]
		4.5960	Juncu [36]
		4.6006	Present

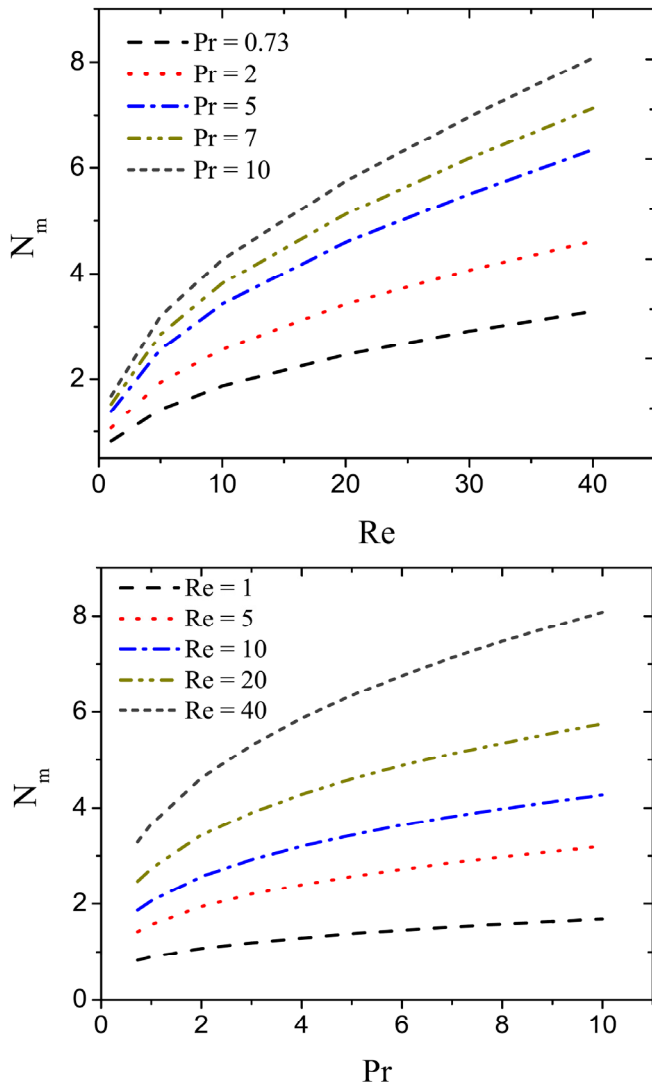


Fig. (6). Dependence of mean Nusselt number N_m on Re and Pr .

In the absence of exact solution, the rate of convergence of the results (drag coefficient C_D , pressure at rear stagnation point $p(0,0)$ and mean Nusselt number N_m) are tested by forming divided differences $d(C_D)/dh$,

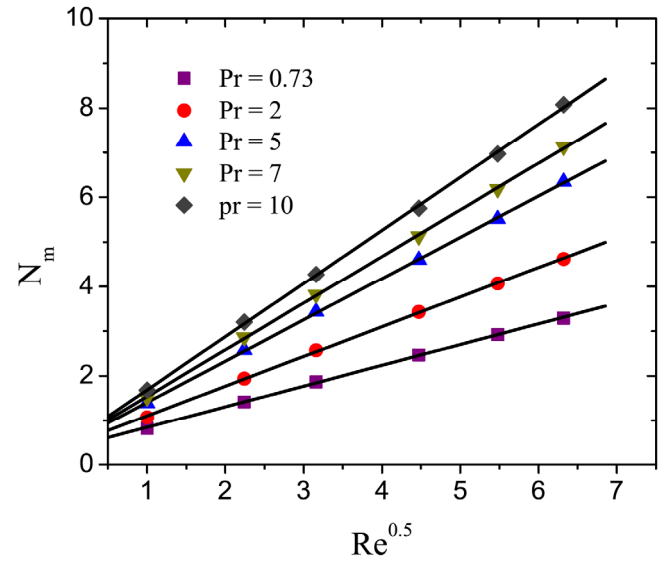


Fig. (7). Linear dependance of mean Nusselt number N_m on \sqrt{Re} .

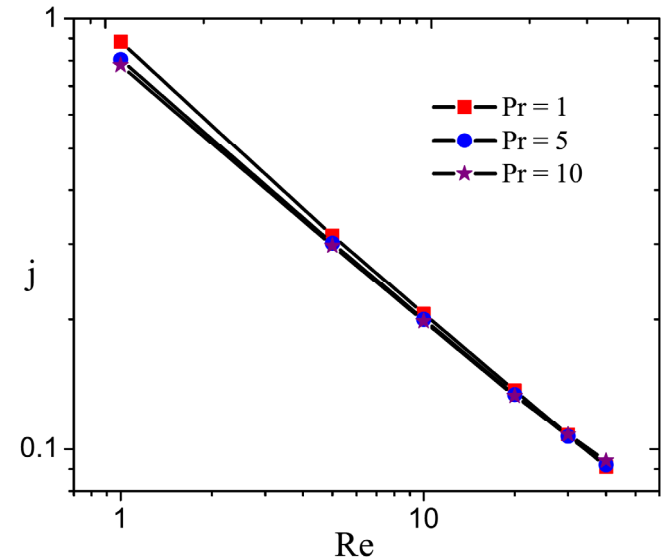


Fig. (8). Colburn heat transfer factor (j) as a function of Re at different Pr .

$dp(0,0)/dh$ and $d(N_m)/dh$ for $Re = 40$ with respect to step sizes h of the data in Table 1. The decay of $d(C_D)/dh$, $d(p(0,0))/dh$ and $d(N_m)/dh$ as function of h is presented in Fig. (10) on log-log scale. Here, the value of 'h' in x-axis is taken as the average of step sizes of the grids corresponding to the divided differences. The slopes of the curves in Fig. (10) are in line with the dotted line of $O(h^3)$. This shows that $d(C_D)/dh$, $dp(0,0)/dh$, $d(N_m)/dh \rightarrow 0$ at the rate of $O(h^3)$ and hence the presented results are fourth order accurate. Here we have stopped our computations with the finest grid of 128×128 in which fourth order accuracy is maintained for momentum, pressure Poisson and energy equations. The increase of grid points/decrease of step size h may degrade the accuracy of the results [41].

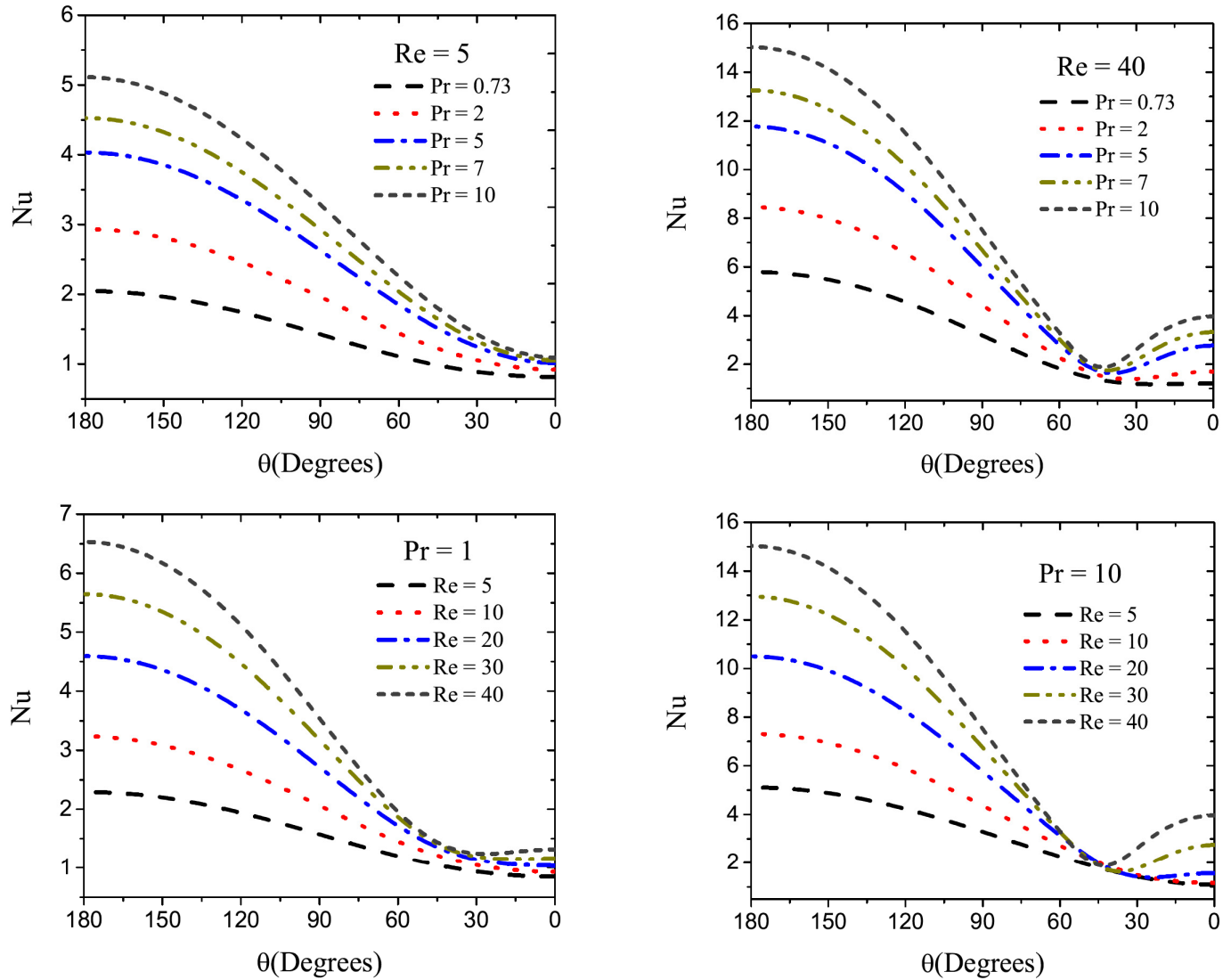


Fig. (9). Angular variation of local Nusselt number Nu on the surface of the cylinder for different Re and Pr .

The fourth order compact scheme is combined with multigrid technique to enhance convergence rate so that CPU time can be minimized. Although multigrid methods are well established with first and second order discretization methods its combination with higher order compact schemes for coupled Navier-Stokes equations are not found in the literature especially with regard to cylindrical polar geometry. In order to verify the effect of the multigrid method on the convergence of the Point Gauss-Seidel iterative method while solving the resulting algebraic system of equations, the solution is obtained from different multigrids starting with five grids 8×8 , 16×16 , 32×32 , 64×64 and 128×128 and by omitting each coarser grid until it reaches single-grid 128×128 . The computations are carried out on AMD dual core Phenom-II X2 555 (3.2 GHz) desktop computer. To verify the effect of multigrid method on restriction operators, the following nine point restriction (full weighting) operator [25] is also used in addition to the injection operator.

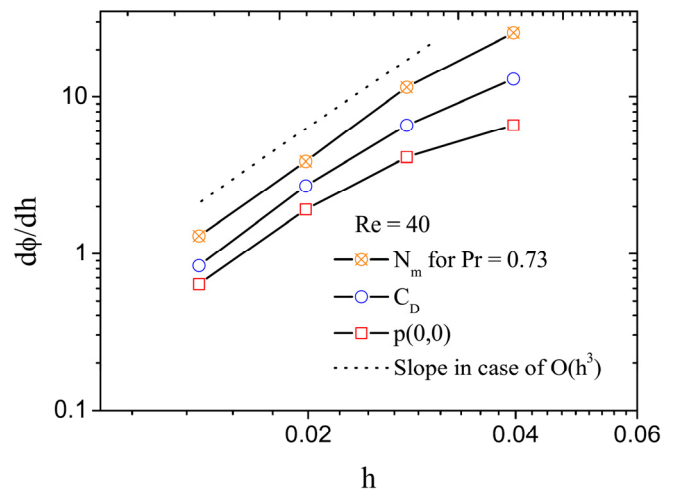


Fig. (10). Decay of $\frac{d\phi}{dh}$ as a function of h where $\phi = C_D, p(0,0), N_m$. Here the values of $d(N_m)/dh$ and $d(C_D)/dh$ are respectively multiplied by 3 and 1.5 to avoid overlapping.

$$(R_k^{k-1}u^k)_{i+1,j+1} = \frac{1}{4}u_{2i+1,2j+1}^k + \frac{1}{8}[u_{2i+2,2j+1}^k + u_{2i+1,2j+2}^k + u_{2i,2j+1}^k + u_{2i+1,2j}^k] + \frac{1}{16}[u_{2i+2,2j+2}^k + u_{2i,2j+2}^k + u_{2i+2,2j}^k + u_{2i,2j}^k]$$

This experiment is done with full weighting and injection operators for Navier-Stokes equations at $Re = 20$. The CPU time (in minutes) taken in different multi-grids and single-grid are presented for Navier-Stokes equations at $Re = 20$ in the Table 6. It is clear from the Table 6 that full weighting restriction operator takes slightly more CPU time than injection operator and the multigrid method with coarse grid correction is very effective in enhancing the convergence rate even when it is combined with higher order compact scheme.

Table 6. Effect of the Multigrid Method on the Restriction Operator for $Re = 20$

No. of Grids	Fine Grid	Coarsest Grid	CPU Time (Min)	
			Nine Point	Injection
1	128 ²	128 ²	8.2688	8.2688
2	128 ²	64 ²	8.7746	8.7628
3	128 ²	32 ²	4.6254	4.6051
4	128 ²	16 ²	4.5220	4.4817
5	128 ²	8 ²	4.5109	4.4694

ACKNOWLEDGMENT

No acknowledgements in our paper.

CONFLICT OF INTEREST

No conflict of interest.

REFERENCES

[1] Gupta MM. High accuracy solutions of incompressible Navier-Stokes equations. *J Comput Phys* 1991; 93: 343-59.

[2] Li M, Tang T, Fornberg B. A compact fourth-order finite difference scheme for the steady incompressible Navier-Stokes equations. *Int J Num Meth Fluids* 1995; 20: 1137-51.

[3] Spatz WF, Carey GF. Higher order compact scheme for the steady stream-function vorticity equations. *Int J Nume Meth Engg* 1995; 38: 3497-512.

[4] Dipankar A, Sengupta TK. Flow past a circular cylinder in the vicinity of a plane wall. *J Fluids Struct* 2005; 20: 403-23.

[5] Iyengar SRK, Manohar RP. High order difference methods for heat equation in polar cylindrical coordinates. *J Comput Phys* 1988; 72: 425-38.

[6] Jain MK, Jain RK, Krishna M. A fourth-order difference scheme for quasilinear Poisson equation in polar coordinates. *Commun Num Meth Engg* 1994; 10: 791-7.

[7] Lai MC. A simple compact fourth-order Poisson solver on polar geometry. *J Comp Phys* 2002; 182: 337-45.

[8] Ray RK, Kalita JC. A transformation-free HOC scheme for incompressible viscous flows on nonuniform polar grids. *Int J Num Meth Fluids* 2010; 62: 683-708.

[9] Sanyasiraju YVSS, Manjula V. Flow past an impulsively started circular cylinder using a higher-order semi compact scheme. *Phys Rev E* 2005; 72: 016709.

[10] Sengupta TK, Ganeriwal G, De S. Analysis of central and upwind compact schemes. *J Comp Phys* 2003; 192: 677-94.

[11] Ghia U, Ghia KN, Shin CT. High-Re solutions for incompressible flow using Navier-Stokes equations and a multigrid method. *J Comp Phys* 1982; 48: 387-411.

[12] Fuchs L, Zhao HS. Solution of three-dimensional viscous incompressible flows by a multi-grid method. *Int J Num Meth Fluids* 1984; 4: 539-55.

[13] Vanka SP. Block-implicit multigrid solution of Navier-Stokes equations in primitive variables. *J Comp Phys* 1986; 65: 138-58.

[14] Juncu GH, Mihail R. Numerical solution of the steady incompressible Navier-Stokes equations for the flow past a sphere by a multigrid defect correction technique. *Int J Num Meth Fluids* 1990; 11: 379-95.

[15] Brandt A, Yavneh I. On multigrid solution of high-Reynolds incompressible entering flows. *J Comp Phys* 1992; 14: 151-64.

[16] Brandt A, Yavneh I. Accelerated multigrid convergence and high-Reynolds recirculation flows. *SIAM J Sci Comput* 1993; 14: 607-26.

[17] Atlas I, Burrage K. A high accuracy defect-correction multigrid method for the steady incompressible Navier-Stokes equations. *J Comp Phys* 1994; 114: 227-33.

[18] Gupta MM, Kouatchou J, Zhang J. Comparison of second and fourth order discretizations for the multigrid Poisson solver. *J Comp Phys* 1997; 132(2) : 226-32.

[19] Gupta MM, Kouatchou J, Zhang J. A compact multigrid solver for convection-diffusion equations. *J Comp Phys* 1997; 132: 123-9.

[20] Zhang J. Accelerated multigrid high accuracy solution of the convection-diffusion equations with high Reynolds number. *Num Meth Par Diff Eqns* 1997; 13: 77-92.

[21] Pardhanani AL, Spatz WF, Carey GF. A stable multigrid strategy for convection-diffusion using high order compact discretization. *Elec Trans Num Annual* 1997; 6: 211-23.

[22] Karaa S, Zhang J. Convergence and performance of iterative methods for solving variable coefficient convection-diffusion equation with a fourth-order compact difference scheme. *Comp Maths Appls* 2002; 44: 457-79.

[23] Zhang J. Numerical simulation of 2D square driven cavity using fourth-order compact finite difference schemes. *Comp Maths Appls* 2003; 45: 43-52.

[24] Briley WR. A numerical study of laminar separation bubbles using Navier-stokes equations. *J Fluid Mech* 1971; 47: 713-36.

[25] Wesseling P. Report NA-37 elft University of Technology The Netherlands 1980.

[26] Dennis SCR, Chang GZ. Numerical solution for study flow past a circular cylinder at Reynolds numbers up to 100. *J Fluid Mech* 1970; 42: 471-89.

[27] Fornberg B. A numerical study of steady viscous flow past a circular cylinder. *J Fluid Mech* 1980; 98: 819-55.

[28] He X, Doolen G. Lattice Boltzmann method on curvilinear coordinates system: flow around a circular cylinder. *J Comp Phys* 1997; 134: 306-15.

[29] Niu XD, Chew YT, Shu C. Simulation of flows around an impulsively started circular cylinder by Taylor series expansion and least squares-based lattice Boltzmann method. *J Comp Phys* 2003; 188: 176-93.

[30] Tritton DJ. Experiments on the flow past a circular cylinder at low Reynolds numbers. *J Fluid Mech* 1959; 6: 547-67.

[31] Kramers HA. Heat transfer from spheres in flowing media. *Physica* 1946; 12: 61-80.

[32] Vander Hegge Zijnen BG. Modified correlation formulae for the heat transfer by natural and forced convection from horizontal cylinders. *Appl Sci Res* 1956; A6: 129-40.

[33] Dennis SCR, Hudson JD, Smith N. Steady laminar forced convection from a circular cylinder at low Reynolds numbers. *Phys Fluids* 1968; 11: 933-40.

[34] Lange CF, Durst F. Momentum and heat transfer from a circular cylinder in laminar crossflow at $10^{-4} \leq Re \leq 200$. *Int J Heat Mass Transfer* 1998; 41: 3409-30.

[35] Kurdyumov VN, Fernandez E. Heat transfer from a circular cylinder at low Reynolds numbers. *ASME J Heat Transfer* 1998; 120: 72-5.

[36] Juncu GH. Conjugate heat/mass transfer from a circular cylinder with an internal heat/mass source in laminar crossflow at low Reynolds numbers. *Int J Heat Mass Transfer* 2005; 48: 419-24.

- [37] Dhiman AK, Chhabra RP, Sharma A, Eswarn V. Effects of Reynolds and Prandtl numbers on heat transfer across a square cylinder in the steady flow regime. *Num Heat Trans, Part A: Appls* 2006; 49:7: 717-31.
- [38] Dennis SCR, Walker JDA, Hudson JD. Heat transfer from a sphere at low Reynolds numbers. *J Fluid Mech* 1973; 40: 273-83.
- [39] Prosenjit B, Kirit K. Effect of freestream isotropic turbulence on heat transfer from a sphere. *Phys Fluids* 2008; 20: 073305.
- [40] Baranyi L. Computation of unsteady momentum and heat transfer from a fixed circular cylinder in laminar flow. *J Comp Appl Mech* 2003; 4: 13-25.
- [41] Spatz WF, Carey GF. Iterative and parallel performance of high-order compact systems. *SIAM J Sci Comput* 1998; 19(1): 1-14.

Received: September 3, 2011

Revised: October 31, 2011

Accepted: November 22, 2011

© Raju and Sekhar; Licensee *Bentham Open*.

This is an open access article licensed under the terms of the Creative Commons Attribution Non-Commercial License (<http://creativecommons.org/licenses/by-nc/3.0/>) which permits unrestricted, non-commercial use, distribution and reproduction in any medium, provided the work is properly cited.